Reprinted from The Journal of Physical Chemistry, 1993, 97.


# Adsorption and Decomposition of $CF_3I$ on Clean and Iodine-Precovered Ag(111)

**Miguel E. Castro, Laura A. Pressley, J. Kiss,† Eddie D. Pylant, S. K. Jo, X.-L. Zhou, and J. M. White***

*Department of Chemistry and Biochemistry, The University of Texas at Austin, Austin, Texas 78712*

*Received: December 9, 1992; In Final Form: May 13, 1993*

To enhance our understanding of the thermal interactions of fluorocarbons with transition-metal surfaces, $CF_3I$ was adsorbed on clean and iodine-precovered Ag(111) and studied by temperature-programmed desorption (TPD), X-ray photoelectron spectroscopy (XPS), ultraviolet photoelectron spectroscopy (UPS), and Auger electron spectroscopy (AES). On clean Ag(111) at 105 K, dissociative adsorption dominates at low coverages and molecular adsorption at high coverages. Dissociation involves C–I bond cleavage; there is no evidence for C–F cleavage, even during TPD. While multilayer desorption peaks near 118 K, chemisorbed $CF_3I$ desorbs in a sharp peak at 126 K with a high-temperature shoulder near 145 K. The only other detectable desorption products are $CF_3$(g) and I(g), which desorb at 300 and 830 K, respectively. In the presence of low coverages of I(a), less $CF_3$ and more $CF_3I$ desorbs. When the surface I/Ag ratio is 0.33 ($\sqrt{3}\times\sqrt{3}R30°$ structure), the dissociation channel is completely suppressed. The influence of atomic iodine is discussed in terms of combined electronic and site blocking effects.

## 1. Introduction

Recently, the chemistry of halocarbons has received considerable attention. Fluorocarbons are important lubricants in aerospace engineering, are important atmospheric pollutants, and play an important technological role in the etching of silicon-based semiconductors.[1-7]

There have been relatively few surface science studies of $CF_3I$ on metals. Dyer and Thiel[8] studied $CF_3I$ on Ru(100) and found that $CF_3$, $CF_2$, CF, F, and Ru–I desorbed during TPD. They concluded that $CF_3I$ decomposes on Ru(100) by C–I bond scission and that C–F bond cleavage occurs during heating. On Ni(100), Jones and Singh[9] came to similar conclusions, except C–F scission was less likely. Myli and Grassian,[10] based on TPD and FTIR, concur and find that $CF_3$ desorbs as a radical at 315 K while atomic iodine desorbs above 900 K. On Pt(111),[11] $CF_3I$ decomposition involves at least two channels which lead to the desorption of $CF_3$ and $CF_2$ radicals.

In this paper, we report on the adsorption and thermal reactions of $CF_3I$ on Ag(111) using temperature-programmed desorption (TPD), Auger electron spectroscopy (AES), ultraviolet photoelectron spectroscopy (UPS), and X-ray photoelectron spectroscopy (XPS). We find two reaction channels: (1) the molecular desorption channel is dominated by the desorption of $CF_3I$ at 125 and 145 K, and (2) the decomposition channel involves C–I bond scission and there is no evidence for C–F bond scission. $CF_3$ (a) desorbs as a radical around room temperature. Atomic iodine desorbs around 830 K. We also studied the effect of preadsorbed iodine, finding that the TPD of $CF_3I$ is sensitive to the structure of the iodine adlayer. Preadsorbed iodine also inhibits the decomposition of $CF_3I$. A model involving site blocking and electronic effects is presented, which accounts for the effect of I(a).

## 2. Experimental Section

All experiments were carried out in an ultrahigh-vacuum chamber described elsewhere.[12a] Briefly, the chamber is equipped with a quadrupole mass spectrometer (UTI 100C) for temperature-programmed desorption (TPD) and residual gas analysis (RGA) and a double pass cylindrical mirror analyzer (PHI 15-255GAR) for Auger electron spectroscopy (AES), and photoelectron measurements. A VG Instruments X-ray source for X-ray photoelectron spectroscopy (XPS) and a homemade ultraviolet He I and He II source for ultraviolet photoelectron spectroscopy (UPS) measurements are also available. The chamber is pumped with an ion pump and auxiliary titanium sublimation and 170 L/s turbomolecular pumps.

The typical base pressure during experiments was $2.5 \times 10^{-10}$ Torr. Substrate temperatures were measured using a chromel–alumel thermocouple welded to a tantalum loop inserted into a hole drilled in the edge of the crystal. The sample could be cooled, by attachment to a liquid nitrogen reservoir, to 105 K and resistively heated to 1000 K. It was cleaned by cycles of $Ar^+$ ion sputtering and annealing to 675 K until no impurities were detected by AES.

For the TPD measurements, the sample was rotated about 20° away from the line-of-sight position with respect to the mass spectrometer. This was done to minimize the influence on the adsorbate of electrons from the mass spectrometer filament. XP spectra were obtained using Mg K$\alpha$ radiation at 1253.6 eV and an analyzer pass energy of 50 eV. XPS scan windows were about 10 eV wide, and data collection time was about 15 min. Core level binding energies were referenced to the Ag($3d_{5/2}$) photoelectron peak centered at 367.9 eV (peak width at half-maximum, $\Delta E_{1/2}$, is 1.97 eV). Binding energy uncertainties are ~0.3 eV.

$CF_3I$ (PCR Research Chemicals Inc., 99.0% pure) was purified by several freeze–pump–thaw cycles and its purity verified by mass spectroscopy. $CF_3I$ was dosed at 105 K through a directed microcapillary array placed about 0.50 cm from the sample. The background $CF_3I$ partial pressure ($\Delta P$) rise was $1 \times 10^{-10}$ Torr with the sample turned away from the doser. The exposures, although very reproducible, are not known in Langmuirs because there is a molecular flux enhancement of approximately 100 (with respect to background $CF_3I$ partial pressure rise) when the surface is positioned in front of the doser. Dosing times are used as a reliable, but relative, measure of exposure.

Absolute coverages of iodine on the Ag(111) surface were determined using calibrated AES spectra. Calibration was done as follows: At room temperature, the Ag(111) was exposed to 1000 langmuirs of $CH_3I$; there is dissociative adsorption and ethane desorption leaving an atomic I/Ag ratio of 0.33 and an ordered $\sqrt{3}\times\sqrt{3}R30°$ LEED pattern.[12b] Using the measured

* To whom correspondence should be addressed.
† Permanent address: Reaction Kinetics Research Group of the Hungarian, Academy of Sciences, University of Szeged, P.O. Box 105, H-6701, Szeged, Hungary.

0022-3654/93/2097-8476$04.00/0 

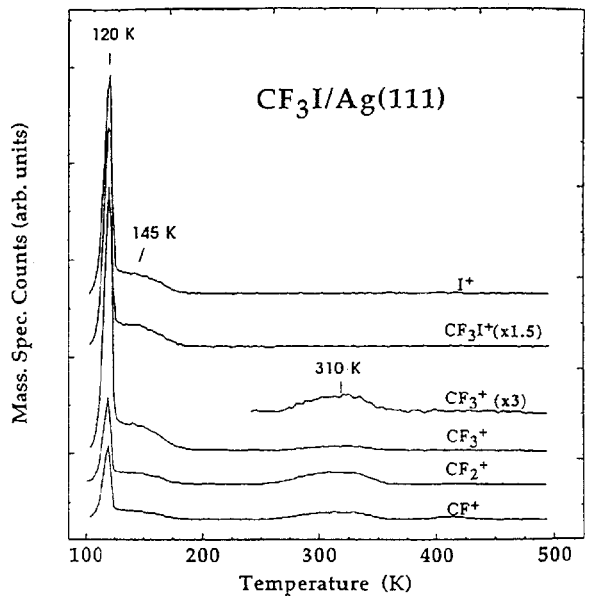


**Figure 1.** Temperature-programmed desorption spectra for a 1 ML coverage of $CF_3I$ on Ag(111) at 105 K.

I(521 eV) to Ag(3512 eV) peak-to-peak ratio for this coverage, and assuming a linear correlation, we calculated other I(a) coverages.

## 3. Results and Discussion

**3.1. TPD.** Figure 1 shows TPD spectra after a saturation (>50 s) $CF_3I$ exposure on Ag(111) at 105 K. Several ion intensities are shown: $CF^+$ ($m/e$ = 31), $CF_2^+$ ($m/e$ = 50), $CF_3^+$ ($m/e$ = 69), $I^+$ ($m/e$ = 127), and $CF_3I^+$ ($m/e$ = 196). Below 500 K, the $I^+$ signal tracks the parent molecule desorption peaks at 126 and 145 K; it is attributed to $CF_3I$ fragmentation in the mass spectrometer. In the same way, $CF_n^+$ fragments ($n$ = 1,2,3) track the parent below 200 K. However, the peaks at 310 K must come from another source since no I-containing fragments are found and since the relative intensities of the $CF_n^+$ fragments ($CF_2^+ > CF^+ > CF_3^+$) differ from those below 200 K ($CF_3^+ > CF_2^+ > CF^+$). There is no evidence for C–F bond scission or C–C bond formation in TPD or XPS (see section 3.2), so we ascribe the 310 K peaks to $CF_3$ radical desorption resulting from $F_3C$–Ag bond breaking. Consistent with $CF_3$ desorption from Ru(100)[8] and Pt(111),[1] the strongest ion signal is $CF_2^+$. Signals corresponding to $F_2$ ($m/e$ = 38), $C_2F_6$ ($m/e$ = 118), or $CF_4$ ($m/e$ = 78) halocarbons were searched for but not found.

Figures 2 and 3 show the TPD of $CF_2^+$ and $I^+$, respectively, as a function of exposure time. We use the $CF_2^+$ mass spectrometer signal to monitor desorption of both the parent $CF_3I$ below 200 K and $CF_3$ radicals near 300 K. For very low exposures, $CF_3$ radicals desorb in a peak centered around 345 K. As the dose increases, this peak broadens and shifts to lower temperatures. Since there is no evidence in TPD or XPS for C–F bond cleavage (see below), the shift is attributed to first-order desorption with repulsive lateral interactions rather than second-order desorption.[13,14] The $CF_3$ desorption saturates for exposures greater than 50 s. The activation energy, $E_a$, for $CF_3$ desorption was calculated using peak width analysis.[15a] Due to lateral repulsions, it is strongly dependent on $CF_3$(a) coverage. In the low coverage limit, $E_a$ is around 16 kcal/mol, whereas in the high coverage limit, it falls to around 5.5 kcal/mol.

Turning to parent desorption, a peak centered around 145 K begins to develop in the $CF_2^+$ TPD spectra for exposures longer than 15 s. Above 25 s, this is accompanied by a sharp peak centered at 126 K. Both are saturated for exposures longer than 50 s. These two peaks are attributed to the desorption of $CF_3I$

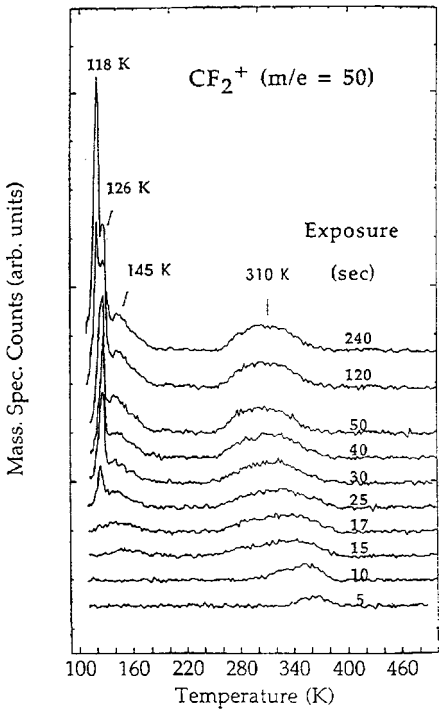


**Figure 2.** $CF_2^+$ TPD spectra for $CF_3I$/Ag(111). Exposure times are indicated.

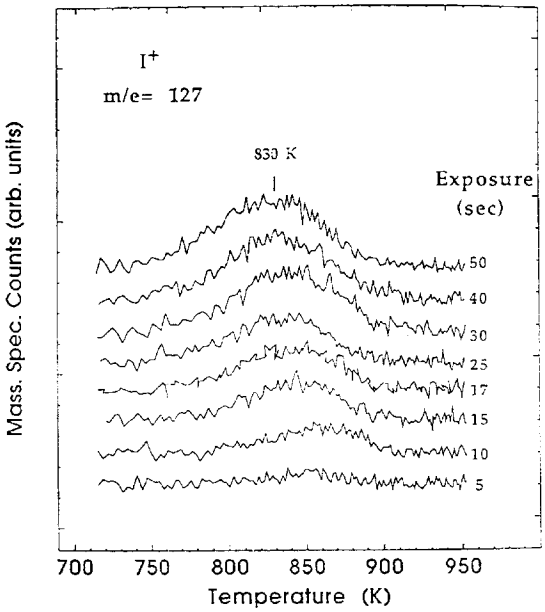


**Figure 3.** $I^+$ TPD spectra for $CF_3I$/Ag(111). Exposure times are indicated.

bound to Ag, i.e., chemisorbed. The desorption state at 140 K is not the result of recombination of $CF_3$(a) and I(a). Below, we support this assignment with F(1s) XPS data. The $E_a$ for the $CF_3I$ species desorbing from the 126 K TPD peak was calculated to be around 15.2 kcal/mol by using the same method described above. For exposures of 120 s or more, there is a peak at 118 K, attributed to the desorption of $CF_3I$ multilayers. On Pt(111), Liu et al.[11] found multilayer desorption peaking at 100 K. Since our sample temperature was no lower than 105 K, we were unable to observe the full width of the multilayer desorption.

Turning to Figure 3, between 750 and 900 K, I(a) desorbs in a broad peak which shifts to lower temperatures with increasing $CF_3I$ exposure time. As discussed elsewhere,[15b] these spectra are attributed to atomic I desorption with strong lateral repulsions. The highest coverage yields an atomic I to atomic Ag ratio of

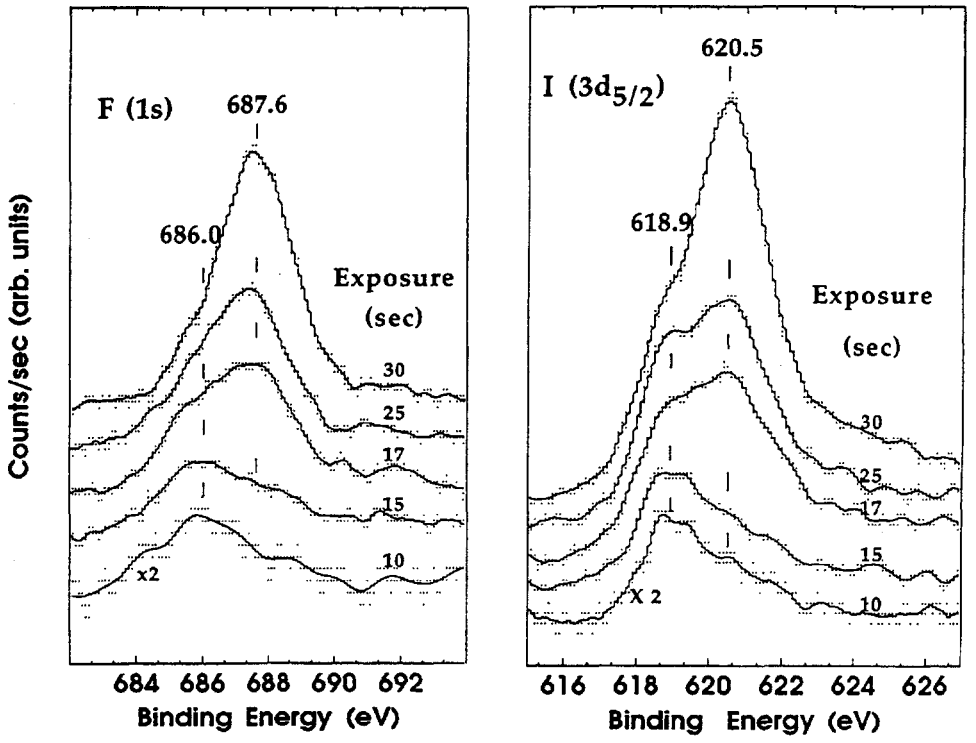


**Figure 4.** F(1s) and I($3d_{5/2}$) XPS (left and right panels, respectively) as function of $CF_3I$ exposure time at 105 K.

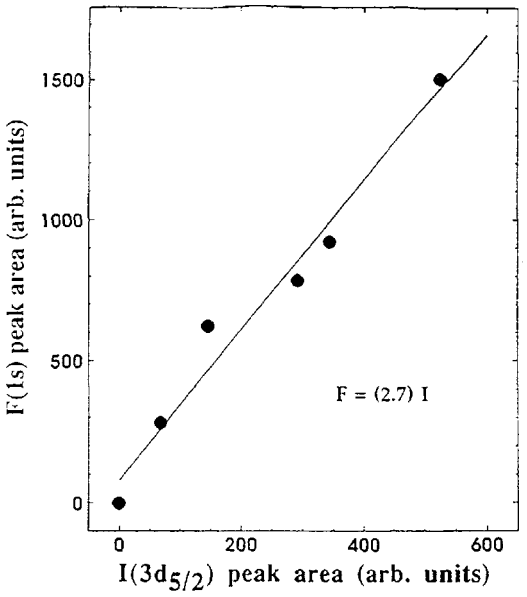


**Figure 5.** F(1s) XPS peak area as a function of XPS I($3d_{5/2}$) peak area. Peak areas are obtained from spectra in Figure 4.

0.12:1 (atomic I/Ag = 0.12), calculated as described in section 2,[12b,16,17] using the measured AES I/Ag peak-to-peak ratio.

**3.2. Photoelectron Spectroscopy Measurements. 3.2.1. Coverage Dependence.** The F(1s) (left panel) and I(3d5/2) (right panel) XP spectra as functions of $CF_3I$ exposure time on Ag(111) at 105 K are shown in Figure 4. To avoid multilayers altogether, exposure times were limited to 30 s. The F(1s) versus the I($3d_{5/2}$) XPS peak areas, which have been corrected for differences in ionization cross section using sensitivity factors,[18a] are shown in Figure 5. The slope of this plot 2.7 ± 0.5, lies near the stoichiometric value of 3 for $CF_3I$ and indicates minimal loss of iodine or fluorine to the gas phase upon $CF_3I$ adsorption.

We now concentrate on the interpretation of the F(1s) and I($3d_{5/2}$) XP spectra, each characterized by two peaks. The I($3d_{5/2}$) peaks are centered at 618.9 and 620.5 eV. The lower binding energy (BE) is assigned to I(a) to bound to Ag,[15] supporting an adsorption model involving some C–I scission upon adsorption at 105 K. The 620.5-eV peak continues to grow with increasing exposure time up to exposures for which molecular $CF_3I$ desorption is observed in TPD (see Figure 2). Correlating with coverage-dependent TPD spectra in Figures 2 and 3, we attribute this peak to the accumulation of $CF_3I$(a). Turning to F(1s), consistent with the above assignments, we assign the peak at 686.0 and 687.6 eV BE to $CF_3$(a) and $CF_3I$(a), respectively. Further evidence for this assignment is discussed in section 3.2.2.

Significantly, XPS shows evidence for $CF_3I$(a), $CF_3$(a), and I(a) for all exposures, including the smallest (10 s). This suggests that at least two types of Ag(111) sites are involved. By comparison, there is no evidence for dissociation of $CH_3I$ on Ag(111) at 105 K.[15] It is interesting to note that the I($3d_{5/2}$) and F(1s) photoemission peaks characteristic of I(a) and $CF_3$(a) species are saturated for exposures longer than 30 s. We conclude that the dissociation channel is active during dosing and is saturated for exposures longer than 30 s.

**3.2.2. Temperature Dependence: UPS.** He II difference UP spectra for 0.5 ML of $CF_3I$ on Ag(111) are shown in Figure 6. In each case, the clean Ag(111) spectrum has been subtracted to construct the difference curve. For the spectra shown, the sample was annealed to various temperatures and cooled for analysis. Gas-phase $CF_3I$ UPS studies by Yates et al.[18b] facilitated the molecular orbital assignments of $CF_3I$(a) and $CF_3$(a). The eight gas-phase binding energies are shown in Figure 6. Atomic iodine was not observed by UPS, perhaps because no more than 6% of monolayer I coverage was involved. All orbital assignments are referenced to the Fermi level.

Curve a in Figure 6 is for a clean Ag(111) surface. Upon adsorption of 0.5 ML of $CF_3I$ at 105 K (curve b), very distinct new features appear. The lowest BE peak at 4.6 eV corresponds to the removal of an electron from the 4e molecular orbital, which is dominated by I 5p lone pair electrons. The 6.6-eV BE ($4a_1$) corresponds to ionization from the C–I bonding orbital. The peaks at 9.3 ($1a_2$, 3e) and 10.4 eV (2e) BE correspond to the ionization of molecular orbitals associated with the fluorine 2p lone pair electrons. Near 12 eV, there is intensity (very weak) which corresponds to ionization of the $3a_1$ molecular orbital, which has significant F(2p) and I(5s) character. The band centered at

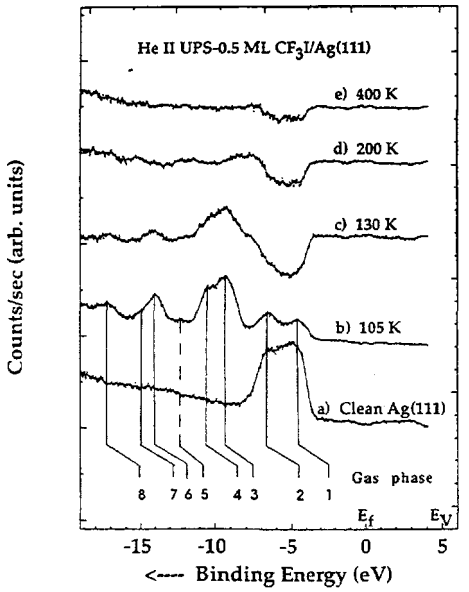


**Figure 6.** He II difference UPS spectra after a 0.5 ML dose of $CF_3I$ on Ag(111) as a function of annealing temperature. The gas-phase molecular orbitals are as follows: (1) 4e; (2) $4a_1$; (3) $1a_2$, 3e; (4) 2e; (5) $3a_1$; (6) $2a_1$; (7) 1e; (8) $1a_1$.

14.0 eV ($2a_1$) is associated with ionization of the C–F bonding molecular orbital. The shoulder at 15.0 eV BE results from ionization from the 1e molecular orbital, which also contains F(2p) and I(5s) character. The highest binding energy band located at 17.3 eV is associated with the C–F bonding molecular orbital, $1a_1$.

Upon annealing to 130 K, which desorbs much of the $CF_3I$, spectral changes occur. Curve c of Figure 6 indicates the retention of the C–F bonds at 130 K; the peaks at 9.3 ($1a_2$, 3e), 10.4 (2e), 14.1 ($2a_1$), and 17.3 ($1a_1$) eV are all present, but with lower intensity.

Annealing to 200 K leaves two new binding energy peaks at 7.39 and 8.61 eV, which we assign to the fluorine 2p lone pair electrons associated with adsorbed $CF_3$. We speculate that the binding energy shift could be due to change in the work function after desorption of $CF_3I$. We did not measure the work function as a function of temperature. The peak separation is 0.2 eV more than their $CF_3I$ counterparts at 9.3 ($1a_2$, 3e) and 10.4 (2e) eV, respectively.

**TABLE I: Binding Energies (eV) for $CF_3I$/Ag(111)**

| | binding/energy (eV) | | |
|---|---|---|---|
| species | F(1s) | I($3d_{5/2}$) | C(1s) |
| $CF_3I$(a) | 687.9 | 620.5 | 291.4 |
| I(a) | | 618.7 | |
| $CF_3$(a) | 686.0 | | 289.2 |

Finally, curve e is the UP spectrum after annealing the sample at 400 K. No fluorine signal at 7.4 and 8.6 eV is apparent, and according to TPD and XPS results, the only remaining species is atomic iodine.

**3.2.3. Temperature Dependence: XPS for Low Coverage.** To gain further insight into the $CF_3I$ decomposition mechanism, we measured F(1s) and I($3d_{5/2}$) XP spectra as functions of annealing temperature for a 15-s $CF_3I$ exposure at 105 K (Figure 7). The XPS sensitivity factor of C(1s) (0.20) is very low compared to F(1s) (1.0) and I($3d_{5/2}$) (5.0); therefore, the C(1s) XPS signal is too weak to be observed at the low coverages. Table I summarizes binding energy assignments for different species. As noted earlier, TPD data in Figure 2 show this exposure, which we estimate to have about 1 $CF_3I$ per surface Ag atom, leads to $CF_3I$(a), $CF_3$(a), and I(a) at 105 K. The I ($3d_{5/2}$) XPS peaks are centered at 618.9 and 620.5 eV (overall half-width of 4.09 eV). After heating to 130 K, the I($3d_{5/2}$) peak narrows ($\Delta E_{1/2}$ = 1.96 eV) and is assignable as a single feature at 618.9 eV (i.e., I(a) dominates). The increase in the I($3d_{5/2}$) 618.7-eV photoemission peak is attributed to the formation for I(a) due to the decomposition of $CF_3I$(a). Since the BE and $\Delta E_{1/2}$ both remain constant upon further heating to 500 K, we conclude that, for this low coverage, the dissociation of $CF_3I$ is complete below 130 K.

The F(1s) XP spectra (Figure 7) are consistent with this interpretation. After heating to 130 K, the peak assigned to molecularly adsorbed $CF_3I$ at 687.6 eV disappears and the one at 686.0 eV, which corresponds to $CF_3$(a), intensifies; this is due

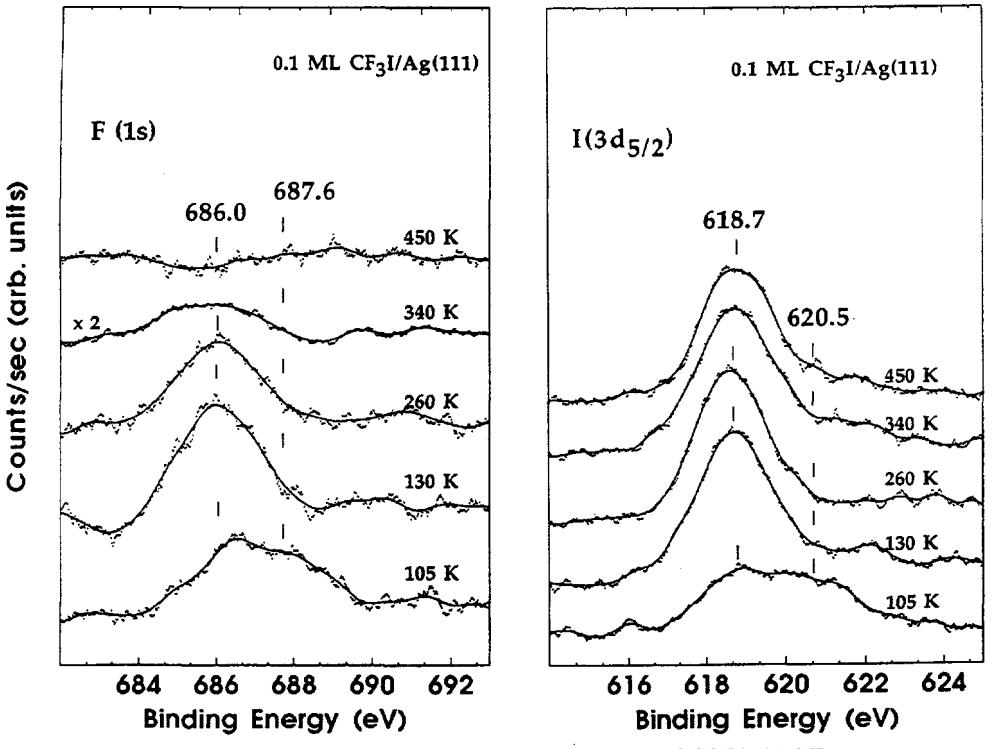


**Figure 7.** F(1s) and I($3d_{5/2}$) XPS as a function of annealing temperature. Initial coverage of $CF_3I$ is 0.1 ML.

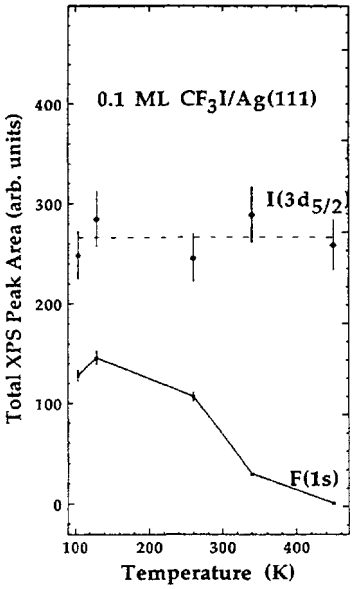


**Figure 8.** Total F(1s) and $I(3d_{5/2})$ XPS peak areas as a function of temperature. Peak areas are obtained from spectra in Figure 7.

to the accumulation of $CF_3(a)$ as a result of the decomposition reaction of $CF_3I(a)$. There is no further BE shift with additional heating, but the total peak area decreases after flashing the substrate above room temperature. Since for a 15 s $CF_3I$ exposure the only fluorine-containing a product in TPD is $CF_3$, we assign the 686.0-eV peak to $CF_3(a)$.

The $I(3d_{5/2})$ and F(1s) XPS peak areas as a function of annealing temperature (unadjusted for sensitivity) are shown in Figure 8. At this low coverage, within experimental error, the total peak area under the $I(3d_{5/2})$ XPS curves remains constant between 105 and 500 K. This is evidence that there is no loss of iodine up to 500 K. The F(1s) total peak area remains constant within experimental error from 105 to 130 K. We conclude that, at very low coverages, the $CF_3I$ that initially adsorbs molecularly undergoes induced decomposition, *not desorption*, upon heating to 130 K. Movement of $CF_3I$ to active sites may be the important process. The F(1s) intensity drops at 260 K, a trend that continues to 450 K, where it is negligible. Consistent with the TPD data, this is further evidence for $CF_3$ desorption. Consistent with TPD, we conclude that 0.1 ML of $CF_3I$ completely dissociates to form $CF_3(a)$ and I(a).

**3.2.4. Temperature Dependence: XPS for High Coverage.** In Figure 9, we show the F(1s), $I(3d_{5/2})$, and C(1s) XP spectra after a 50-s $CF_3I$ dose (0.5 ML) and annealing to indicated temperatures. The C(1s) XPS is characterized by two peaks centered at 289.2 and 291.4 eV. After flashing to 140 K, the peak at 291.4 eV nearly disappears, but the peak at 289.2 eV remains. There is no further BE shift upon heating to 250 K and the signal disappears after flashing to 450 K. We assign the C(1s) peak at 291.4 eV to $CF_3I(a)$, since it is the only TPD product below 200 K. Since the only carbon-containing products in TPD between 200 and 500 K are $CF_3$ radicals, we assign the C(1s) XPS peak at 289.2 eV to adsorbed $CF_3$ species, i.e., a single C-containing species. Consistent with this interpretation, between 200 and 260 K, the F(1s) and $I(3d_{5/2})$ spectra show only single peaks centered at 686.0 eV ($\Delta E_{1/2}$ = 1.98 eV) and 618.9 eV ($\Delta E_{1/2}$ = 2.01 eV), respectively.

The F(1s) XP spectra in Figure 9 can be used to argue against the possibility that the 145 K $CF_3I$ TPD peak is not due to recombination of adsorbeed $CF_3$ and I. Significant F(1s) XPS signal attributed to parent $CF_3I$ remains after annealing to 140 K and readily accounts for the $CF_3I$ TPD peak at 145 K. Therefore, we conclude there are at least two types of adsorbed states for molecular $CF_3I$.

Figure 10 shows XPS areas, uncorrected for sensitivity, as a function of annealing temperature. All the peak areas decrease sharply upon flashing to 145 K, consistent with $CF_3I$ desorption below 140 K. The fractional decrease of the $I(3d_{5/2})$ signal is small compared to those for C and F, a trend which continues, particularly evident in the F case, up to 350 K. This is consistent with significant $CF_3$ *desorption* and *retention* of I(a).

Significantly, the F(1s) and C(1s) peak areas, characteristic of $CF_3(a)$, and the $I(3d_{5/2})$ signal, characteristic of I(a), do not increase after the sample is flashed to 140 K. In addition, the corresponding XPS peak areas for adsorbed $CF_3I$ to decrease with substrate temperatures above 140 K. This indicates that,

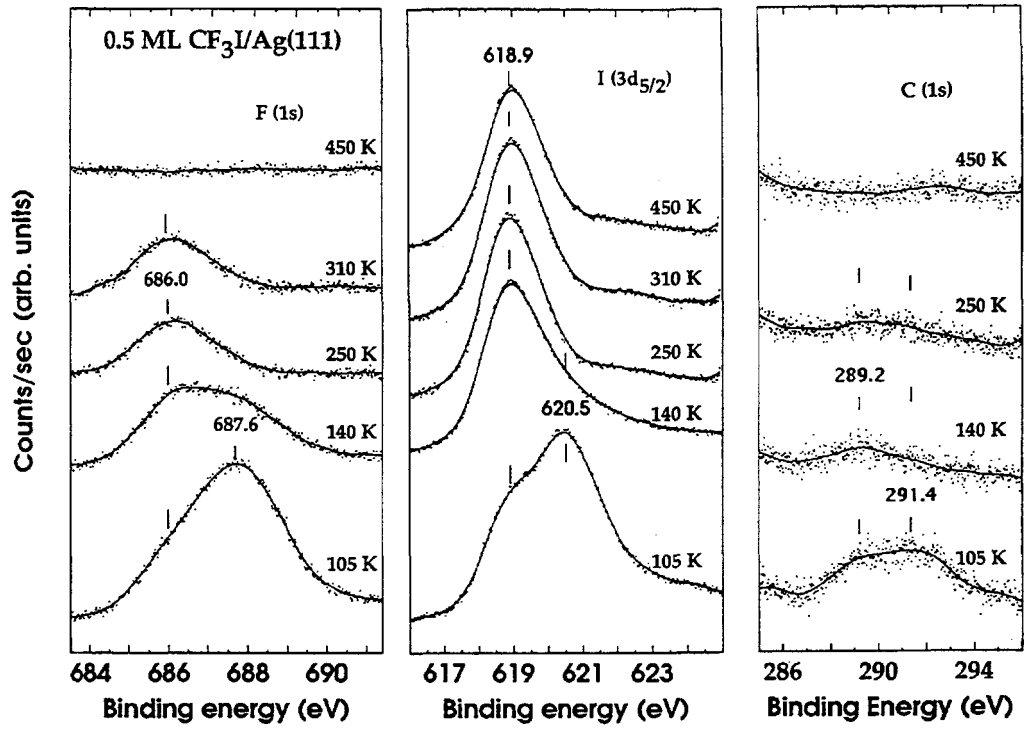


**Figure 9.** F(1s), $I(3d_{5/2})$, and C(1s) XPS as a function of annealing temperature. Initial coverage of $CF_3I$ is 0.5 ML.

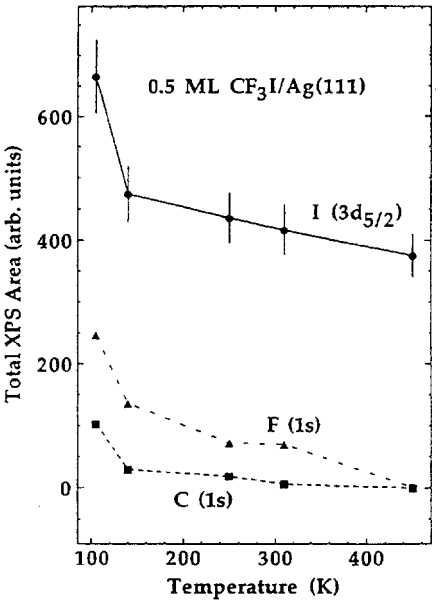


**Figure 10.** Total F(1s) and I($3d_{5/2}$) XPS peak areas as a function of temperature. Peak areas are obtained from spectra in Figure 9.

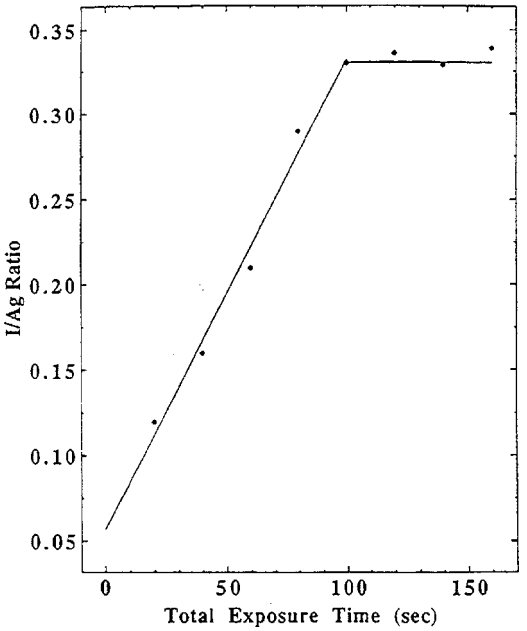


**Figure 11.** I/Ag ratio as a function of total integrated $CF_3I$ exposure time. Each point is taken after a cumulative 20-s dose of $CF_3I$.

at higher coverages, (1) $F_3C$–I scission is complete at 105 K and (2) the remaining (undecomposed) molecular $CF_3I$ desorbs below 250 K, in agreement with TPD results shown in Figure 2.

**3.3. Iodine-Covered Ag(111).** Interesting changes occur when I(a) is preadsorbed. Figure 11 shows how I(a) accumulates with repeated 20-s doses of $CF_3I$ and flashes to 700 K. The experiments were performed as follows: After each 20-s dose, the surface was heated to 700 K to remove the adsorbate fragments, $CF_3I$(a) and $CF_{3(a)}$, leaving I(a). From AES, the first dose of $CF_3I$ gives an I/Ag ratio of 0.12. This spectrum corresponds to approximately a 17-s dose of $CF_3I$ as shown in Figure 2. This iodine-covered surface was subsequently exposed to another 20-s dose of $CF_3I$ and flashed to 700 K, and the AES I/Ag ratio was again determined. The second dose yields an I/Ag ratio of 0.16, and so on. The next three sequential doses each increase the I/Ag ratio by approximately 0.05, reaching a saturation coverage that yields an atomic iodine to atomic silver ratio of 0.33. The I/Ag ratio saturated at 0.33.

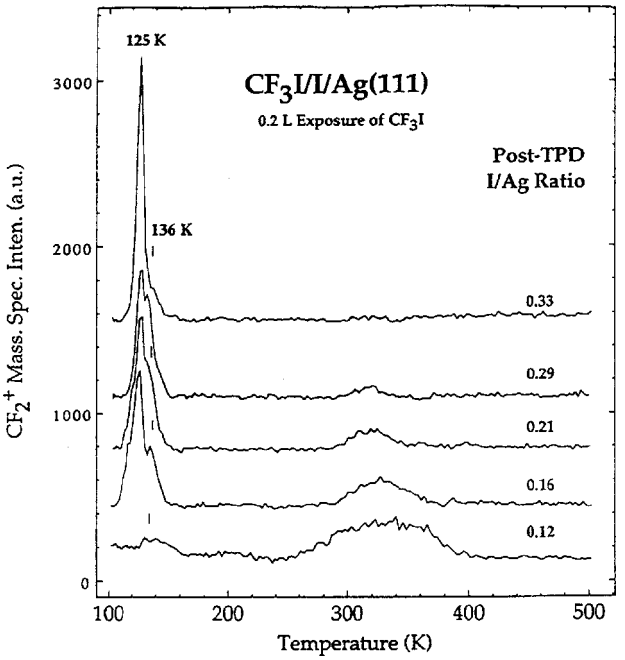


**Figure 12.** Adsorption and decomposition channels of repeated exposures of $CF_3I$. For the bottom curve, a clean Ag(111) surface was dosed with 0.2 langmuir and after TPD, as indicated in the figure, an I/Ag ratio of 0.12 remained. To obtain the second curve from the bottom, the previously remaining iodine (I/Ag ration of 0.12) was exposed to 0.2 langmuir of $CF_3I$ again and after TPD to 500 K, the I/Ag ratio increased to 0.16. This procedure of sequentially dosing on top of the previously remaining iodine was repeated until an iodine-saturated Ag surface was achieved. The I/Ag ratio indicated is the coverage after the respective TPD.

The $CF_2^+$ TPD spectra for various precoverages of I(a) are shown in Figure 12. The peak between 300 and 400 K monitors $CF_3$ radical desorption, whereas the lower temperature peaks monitor parent desorption. Clearly, as the iodine precoverage increases, (1) the high-temperature shoulder of the parent desorption TPD peak is suppressed, (2) the 125 K peak intensities, and (3) the amount of $CF_3$ desorption decreases.

We now discuss the effect of surface iodine on the parent desorption channel (Figure 12). First, we concentrate on the $CF_3I$ TPD spectra for low I/Ag ratios. In TPD after the first dose (bottom curve), $CF_3I$ desorbs in a weak and broad peak centered at 140 K. In TPD after the second dose, there are two prominent peaks—at 125 and 136 K. In subsequent doses, the 136 K peak first increases and then decreases, while the 125 K peak remains nearly constant and then increases as the 136 K peak decreases. We conclude that when I/Ag < 0.29, there is an enhancement of $CF_3I$ desorption at 136 K.

With regard to the $CF_3$ desorption peak around 310 K, it shifts to lower temperatures with increasing iodine precoverage, characteristic of first-order desorption kinetics with strong lateral repulsions. A simple second-order kinetic model is readily discarded because there is no overlap of the high-temperature side of the TPD spectra. From the data in Figure 12, the decrease in the TPD area of the adsorbed $CF_3$ (310 K peak) as a function of I(a) precoverage is plotted in Figure 13 (solid squares). This is good evidence for the suppression of C–I bond scission as a function of I(a) precoverage.

By modeling the $CF_2^+$ TPD peak area as a function of iodine coverage, we estimate the absolute Ag atom ensemble requirement for $CF_3I$ decomposition. In Figure 13, the solid squares are experimental data, whereas the open diamonds and circles are model fits using a simple site blocking model proposed by Campbell et al. The fraction of $CF_3I$ dissociating can be described by[18c]

$$F(CF_3I_{diss}) \propto [r(1-z\theta)^n]/[1+r(1-z\Theta)^n] \qquad (1)$$

where $r$ is the ratio rate of dissociation/rate of desorption for

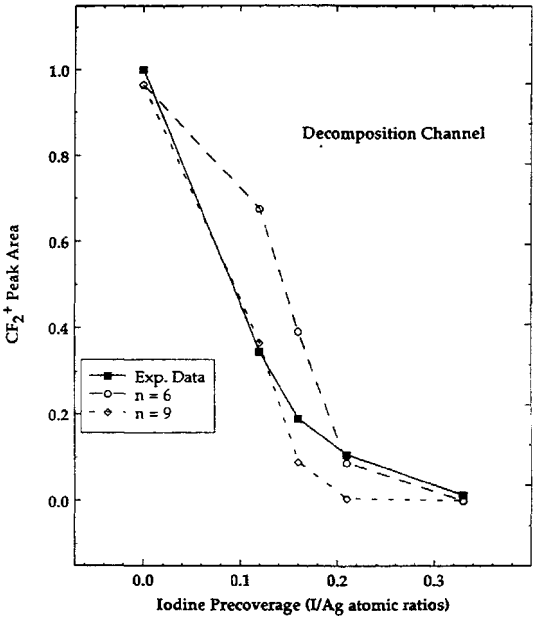


**Figure 13.** Decrease of $CF_2^+$ TPD peak area as a function of iodine precoverage. Solid squares are experimental data, whereas open circles and diamonds are site blocking model fits.

$CF_3I$. It is clear from the XPS data in Figure 4 that the dissociation rate is much higher than the rate for molecular adsorption ($r \gg 1$). The best fit to the data for $r$ gave a value of 27. The number of Ag atoms sterically hindered by each atom of I(a) is represented by the variable $z$. Since the I(a) sits in threefold sites, $z = 3$. $\theta$ is the coverage of I(a), and $n$ is the absolute ensemble size which is defined as the number of additional Ag atoms required for decomposition as for molecular adsorption. From Figure 13, we estimate the absolute ensemble size of Ag atoms required for $CF_3I$ decomposition on Ag(111) to be in the range 6–9, and the fit is generally better for $n = 9$. In passing, we note that Campbell et al. calculated similar values for the dehydrogenation of benzene on Pt(111).[18c]

When $CF_3I$ is dosed into an I(a)-saturated Ag(111) surface (I/Ag ratio of 0.33), several desorption channels are completely suppressed. As the exposure time increases from 20 to 100 s (Figure 14), the TPD of $CF_3I$ simply indicates growth and saturation of a weakly held (125 K) parent molecule. The 100-s dose indicates the growth of the multilayer $CF_3I$ around 115 K. The 136 K TPD peak is absent. Thus, even though a structural model indicates Ag sites are accessible, the decomposition channel (310 K) and the desorption state at 136 K are completely suppressed.

## 4. Conclusion

From all the evidence presented here, low-temperature $CF_3I$ decomposition on Ag(111) occurs exclusively by C–I bond scission to form adsorbed $CF_3$(a) and I(a). There is no evidence for C–F bond scission in either TPD or XPS. This is in contrast to recent studies on more active metals, Ru(100)[8] and Pt(111),[11] where C–I and multiple C–F bond scission is evidenced in TPD. These differences in C–F activation correlate with the differences of these metals in C–H activation; i.e., Ag is inactive compared to Ru and Pt.

The structure of $CF_3I$ on Ag(111) was not determined in this study. However, our XPS measurements indicate only one type of fluorine and one type of iodine. The simplest model, and one intuitively satisfying, involves adsorption with the I toward the surface and the three F atoms symmetrically placed away from the surface, as in $CH_3I$.[15]

In the gas phase, $CF_3I$ has very interesting properties. It has a large electron affinity and rate constant for dissociative electron

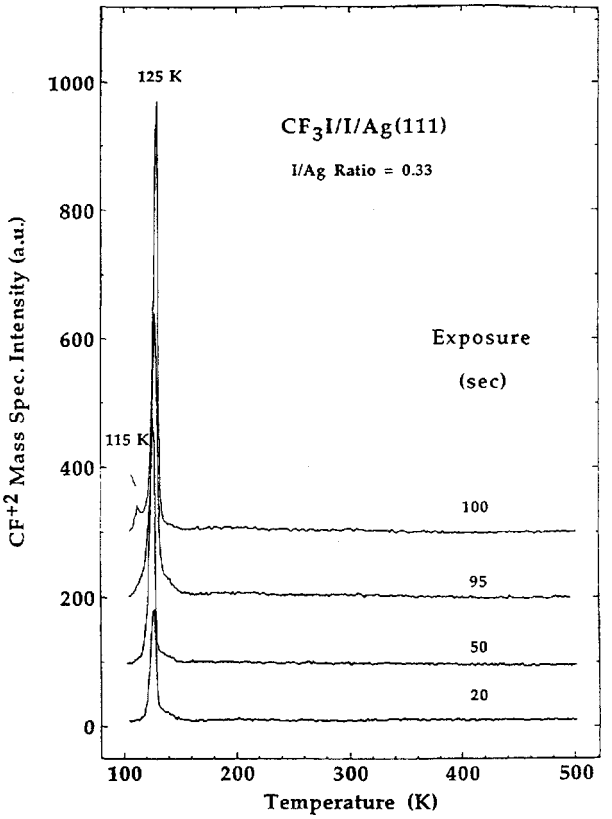


**Figure 14.** $CF_3I$ desorption spectra for a saturated (I/Ag ratio of 0.33) iodine precovered Ag(111) surface as a function of $CF_3I$ exposure time.

attachment.[19,20] The major portion of the excess energy liberated by electron capture appears as translational energy of the fragments.[20-22] Molecular beam measurements of $CF_3I$ colliding with K atoms indicate the formation of K–I and $CF_3$ radicals,[21] but no F–K or C–K bonds. Activation of the C–I bond by potassium was attributed to a long-range harpooning mechanism where electrons are transferred from the electropositive K atoms into the electronegative $CF_3I$ molecule.[21,23] In a surface analog, Zhou et al.[24] reported the activation of the C–Br bond upon exposure to methyl bromide to a Ag(111) surface precovered by potassium at 105 K and interpreted their results in terms of surface harpooning. This previous work with methyl and fluorocarbon halides was one motivation for the present study. However, unlike $CH_3Br$/K/Ag(111), where $CH_3$ fragments are ejected during dosing, we found $CF_3$ is retained. Comparing Ag and K, both have a similar highest occupied band—a half-filled s band—but the ionization potentials are markedly different, 7.576 and 4.349 eV for Ag and K, respectively.[25] This makes an electron-transfer process (harpooning) much more likely for potassium than for silver. Thus, our results are consistent with thermal activation of the $F_3C$–I bond.

It is interesting that $CF_3$(a), unlike $CH_3$,[15] does not recombine; rather, it desorbs as a radical. This interesting result deserves further study; here we only outline possible reasons for the difference. Replacing H with the more electron-withdrawing F will weaken the C–C bond so there is a stronger thermodynamic driving force to form $C_2H_6$. On the other hand, it is striking that the $CF_3$ desorption peak temperature (breaking a C–Ag bond) is only about 40–60 K higher that the $C_2H_6$ desorption peak (simultaneously breaking a C–Ag bond and making a strong C–C bond). The thermodynamic driving force for making $C_2F_6$ is certainly higher than for the desorption of $CF_3$. We conclude that significant kinetic barriers must exist in this channel. Perhaps lateral repulsions among adsorbed $CF_{3(a)}$ species inhibit $C_2F_6$ formation. Sterically, F is larger than H and, electronically, F carries more *net* negative charge than H. The shift toward lower

$CF_3$ desorption peak temperatures with increasing coverage is consistent with this interpretation. A similar interpretation has been given for the desorption of I on Ru(100)[8] and Ag(111).[11]

Partial decomposition of $CF_3I$ at 105 K indicates that $CF_3I$ decomposition is self-inhibited, a phenomenon well-documented in the literature.[26-28] As the coverage of surface species increases, there is a reduction in the number of sites available for $CF_3I$ decomposition. In general, molecular adsorption appears after the saturation of the decomposition channel, but in the present case, molecularly adsorbed $CF_3I$ appears well before saturation of the decomposition channel (see F(1s) and I($3d_{5/2}$) intensities as a function of $CF_3I$ exposure). In addition, the XPS for a 10-s $CF_3I$ exposure suggests that there are plenty of surface sites available for C–I bond scission; $CF_3I$ decomposes quantitatively upon flashing the substrate to 130 K. The fact that all of the $CF_3I$ does not decompose at very low coverages is quite interesting. We conclude that island formation occurs and that a simple site blocking model does not fully account for the decomposition mechanism of $CF_3I$ on Ag(111) at 105 K.

Another possible explanation lies in the kinetics of $CF_3I$ decomposition. It is plausible that C–I scission occurs slowly at 105 K. To test this possibility, we made XPS measurements (not shown) just after the adsorption of $CF_3I$ and up to 30 min later. Comparison of both measurements revealed the same amount of molecularly adsorbed $CF_3I$.

A more satisfying model assumes at least two kinds of sites are involved in the adsorption and decomposition of $CF_3I$ on Ag(111), and one of them is active for C–I bond scission at 105 K, whereas the other requires additional thermal activation. Such a model assumes that $CF_3I$ is not mobile at the adsorption temperature and there is no interconversion between $CF_3I$ on the two proposed Ag sites. This is consistent with the above observations and also accounts for observations in the presence of I(a) precoverage.

Saturation I(a) on Ag(111) corresponds to an I/Ag ratio of 0.33 ($4.80 \times 10^{14}$ iodine atoms/cm$^2$)[16] and a $\sqrt{3}\times\sqrt{3}R30°$ LEED structure.[16,29-33] The iodine atoms occupy 3-fold hollow sites that *do not* have a silver atom underneath, and the distance between the adsorbed iodine atoms is 4.98 Å.[16] Further iodine uptake, without the formation of a second layer, is limited by strong repulsions among the adsorbed adatoms.[15,31,32]

Below saturation, the structure is more complicated. On the basis of LEED intensity analysis, Maglieta et al.[29] have proposed a model in which the iodine atoms occupy 3-fold hollow sites with and without a silver atom underneath. Farrell et al.[30] and Kang et al.[33] have proposed a similar model with a random distribution of iodine atoms over both sites. The populations of these sites depends on coverage and, presumably, on the details of preparation.

The effect of these coverage-dependent iodine structures on the surface chemistry of $CF_3I$, as revealed by our TPD studies, is fascinating. On the clean surface, $CF_3I$ desorbs in a peak centered at 125 K and a high-temperature shoulder around 140 K; the shoulder increases for I/Ag ratios below 0.33 ML, while the 125 K desorption peak area remains constant. But the shoulder is excluded as soon as the saturation I(a) coverage is reached. Citrin has reported that the $\sqrt{3}\times\sqrt{3}R30°$ iodine structure on Ag(111) appears abruptly and exclusively for a saturation iodine coverage.[31,32] We speculate that the high-temperature shoulder involves $CF_3I$ molecules interacting with the 3-fold sites that *do* have a silver atom underneath.

The nature of the adsorbate–substrate interactions that lead to the $CF_3I$ desorption peak at 125 K is difficult to assess. The maximum peak area is independent of iodine precoverages below 0.33. However, since it is the only desorption peak observed when the surface is precovered with an I/Ag ratio of 0.33, we suggest that atomic I in 3-fold sites that *do not* have a silver atom underneath are involved. We suggest that the sharpening of the 125 K TPD peak when I/Ag = 0.33 is a result of a high degree of order and surface unformity.

The electronic effect of submonolayer and a monolayer coverage of iodine on Ag(111) cannot be ignored. Compared to a clean surface, the work function of Ag(111) is 0.35 eV higher for saturation I(a) and the accompanying charge redistribution may also contribute to the suppression of the decomposition probability.

## 5. Summary

Our results can be summarized as follows:

(1) Two channels are involved in the interaction of $CF_3I$ with Ag(111). The molecular desorption channel is dominated by a sharp $CF_3I$ peak at 125 K and a high-temperature shoulder that peaks at about 140 K. The decomposition channel is limited to C–I bond scission, below 130 K, to form $CF_3$(a) and I(a). No evidence for C–F bond scission or C–C bond formation was found in TPD or XPS measurements. $CF_3$(a) desorbs as a radical near room temperature.

(2) The F(1s), I($3d_{5/2}$), and C(1s) XPS binding energies for $CF_3$ adsorbed on Ag(111) are 687.6, 620.5, and 291.4 eV, respectively. The F(1s) and C(1s) binding energies for $CF_3$(a) are 686.0 and 289.2 eV, respectively. The I($3d_{5/2}$) binding energy for I(a) is 618.9 eV.

(3) An iodine adlayer inhibits the decomposition of $CF_3I$, a result attributed to combined electronic and site blocking effects. The absolute ensemble size needed for decomposition of $CF_3I$ was calculated to be in the range 6–9 atoms.

(4) The molecular desorption channel is sensitive to the structure of the iodine adlayer. Submonolayer I(a) increases the amount of $CF_3I$ desorption in the high-temperature shoulder above 125 K, but with a saturated $\sqrt{3}\times\sqrt{3}R30°$ iodine structure, desorption is exclusively in the 125 peak.

**Acknowledgment.** Support by the U.S. Army Research Office is gratefully acknowledged. The authors thank Z.-M. Liu and Professor Charles T. Campbell for stimulating discussions. In addition, L.A.P. acknowledges support by the American Business Women's Association and the Promethium Chapter of Iota Sigma Pi–National Honor Society for Women in Chemistry.

## References and Notes

(1) (a) Robertson, R. M.; Golden, D. M.; Rossi, M. J. *J. Vac. Sci. Technol. B* **1988**, *6*, 1632. (b) Fu, X.; Chen, G.; Ren, C.; Zheng, Y.; Chen, L.; Fang, H.; Yang, J. *Bandaoti Xuebao* **1985**, *6*, 423.

(2) Lin, S. T.; Klabunde, K. J. *Inorg. Chem.* **1985**, *24*, 1961.

(3) Kalbunde, K. J. *J. Fluorine Chem.* **1976**, *7*, 95.

(4) McFeely, F. R.; Yarmoff, J. A.; Beach, P. B. *J. Chem. Phys.* **1988**, *89*, 7609.

(5) McFeely, F. R.; Yarmoff, J. A.; Taleb-Ibrahimi, A.; Beach, P. B. *Surf. Sci.* **1989**, *210*, 429.

(6) Roop, B.; Joyce, S.; Scultz, J.; Steifeld, J. *J. Chem. Phys.* **1985**, *83*, 6012.

(7) Creasy, W. R.; McElvany, S. W. *Surf. Sci.* **1989**, *201*, 59.

(8) Dyer, J. A.; Thiel, P. A. *Surf. Sci.* **1990**, *238*, 169.

(9) Jones, R. G.; Singh, Nagindar, K. *Vacuum* **1988**, *38*, 213.

(10) Myli, K. M.; Grassian, V. H. *Surf. Sci.*, submitted for publication.

(11) Liu, Z. M.; Zhou, X.-L.; Kiss, J.; White, J. M. *Surf. Sci*, submitted for publication.

(12) (a) Koel, B. E.; Peebles, D. E.; White, J. M. *Surf. Sci.* **1983**, *125*, 709. (b) Gerenser, L. J.; Baetzold, R. C. *Surf. Sci.* **1980**, *99*, 259.

(13) Chan, C.-M.; Aris, R.; Weinberg, W. H. *Appl. Surf. Sci.* **1978**, *1*, 360.

(14) Redhead, P. A. *Vacuum*, **1962**, *12*, 203.

(15) (a) Chan, C. M.; Weinberg, W. H. *Appl. Surf. Sci.* **1978**, *1*, 377. (b) Zhou, X.-L.; Solymosi, F.; Blass, P. M.; Cannon, K. C.; White, J. M. *Surf. Sci.* **1989**, *219*, 203.

(16) Forstmann, F.; Berndt, W.; Buttner, P. *Phys. Rev. Lett.* **1973**, *30*, 17.

(17) Davis, L. E.; MacDonald, N. C.; Palmberg, P. W.; Riach, G. E.; Weber, R. E. In *Handbook of Auger Electron Spectroscopy*, 2nd ed.; Physical Electronics Industries: Eden Praire, 1971.

(18) (a) Muilenberg, G. E. In *Handbook of X-ray Photoelectron Spectroscopy*; Perkin-Elmer: Eden Praire, 1979. (b) Yates, B. W.; Tan, K. H.; Bancroft, G. M.; Tse, J. S. *J. Chem. Phys.* **1986**, *85*, 3840. (c) Campbell,

C. T.; Campbell, J. M.; Dalton, P. J.; Henn, F. C.; Rodriguez, J. A.; Seimanides, S. G. *J. Phys. Chem.* **1989**, *93*, 806.
(19) ChristophorouL, G. In *Electron-Molecule Interactions and Their Applications*; Academic Press: New York, 1984.
(20) Walter, C. W.; Lindsay, B. G.; Smith, K. A.; Dunning, F. B. *Chem. Phys. Lett.* **1989**, *154*, 409.
(21) Harland, P. W.; Camon, H. S.; Phillips, L. F.; Brooks, P. R. *J. Chem. Phys.* **1990**, *93*, 1089.
(22) Young, Mark, A.; Pimentel, G. C. *J. Phys. Chem.* **1990**, *94*, 4884.
(23) Brooks, P. R.; Mckillop, J.; Pippen, H.-G. *Chem. Phys. Lett.* **1979**, *66*, 144.
(24) Zhou, X.-L.; Coon, S.; White, J. M. *J. Chem. Phys.*, in press.
(25) Doublas, B.; McDaniel, D. H.; Alexander, J. J. In *Concepts and Models of Inorganic Chemistry*, 2nd ed.; John Wiley & Sons: New York, 1983.
(26) Castro, M. E.; Ahkter, S.; Golchet, A.; White, J. M.; Sahin, T. *Langmuir* **1991**, *7*, 126.
(27) Zhu, X. Y.; Castro, M. E.; Ahkter, S.; White, J. M.; Houston, J. *J. Vac. Sci. Technol. A* **1989**, *7*, 1991.
(28) Zhou, X.-L.; White, J. M. *Chem. Phys. Lett.* **1987**, *142*, 376.
(29) Magliuetta, M.; Zanazzi, E.; Bardi, N.; Sodericher, D.; Jona, F.; Marcus, P. M. *Surf. Sci.* **1982**, *123*, 141.
(30) Farrel, H. H.; Trau, M. M.; Smith, N. V.; Roger, W. A.; Woodruff, D. P.; Johnson, P. D. *Surf. Sci.* **1981**, *102*, 527.
(31) Citrin, P. H.; Eisenberger, P.; Hewitt, R. C. *Phys. Rev. Lett.* **1978**, *41*, 309.
(32) Citrin, P. H.; Eisenberger, P.; Hewitt, R. C. *Surf. Sci.* **1978**, *89*, 28.
(33) Kang, W. M.; Li, C. H.; Yong, S. T. *Solid State Commun.* **1980**, *36*, 149.